High-resolution x-ray-photoemission study of single crystalline $Sr_2CuO_2Cl_2$

T. Böske,* O. Knauff, R. Neudert, M. Kielwein, M. Knupfer, M. S. Golden, and J. Fink
Institut für Festkörper- und Werkstofforschung Dresden, Postfach 270016, D-01171 Dresden, Germany

H. Eisaki and S. Uchida
Department of Superconductivity, University of Tokyo, Bunkyo-ku, Tokyo 113, Japan

K. Okada
Faculty of Education, Yamaguchi University, 1677-1, Yoshida, Yamaguchi 753, Japan

A. Kotani
Institute for Solid State Physics, University of Tokyo, 7-22-1, Rappongi, Minato-ku, Tokyo 106, Japan
(Received 27 January 1997; revised manuscript received 8 April 1997)

$Sr_2CuO_2Cl_2$ contains CuO_2 planes separated by ionic SrCl block layers and can be regarded as a model substance for cuprates concerning many of their physical properties, in particular the dynamics of valence-band holes in a two-dimensional antiferromagnetic background. We present and discuss core-level and valence-band photoemission data. The Cu-$2p$ photoelectron spectrum differs from the spectra of other cuprate compounds, in particular with regard to the parent cuprates of the high-T_c superconductors. The Cu-$2p$ main lines are comprised of more than two peaks with strong satellite emission which exhibits a distinct angular-dependent fine structure. We present calculations of a Cu_5O_{16} cluster within the d-p model and discuss the features in the main line of the Cu-$2p$ photoemission spectrum in terms of the different screening channels available in CuO_2 planes. [S0163-1829(97)05730-5]

I. INTRODUCTION

X-ray-photoemission spectroscopy (XPS) has provided valuable insight into the structure of the occupied electronic states of late-transition-metal compounds, such as the copper dihalides[1] and copper oxides.[2–4] In particular, the detailed shape of the Cu-$2p$ spectra, taken together with cluster calculations delivers an experimental check of the parameters which enter into models used to describe the electronic structure of these strongly correlated materials.

In many formally divalent copper compounds, the Cu-$2p$ spectrum shows a strong satellite feature which is assigned to emission giving rise to mainly a poorly screened $2p^5 3d^9$ final state.[1,4,5] While the attribution of the main line to a well-screened final state in which no d holes reside at the $2p$ core hole site is broadly accepted, the origin of the large width and high binding-energy asymmetry of the Cu-$2p$ main line has been the subject of discussion. In earlier treatments,[1,4,5] the low binding-energy component, i.e., the main line, was discussed in terms of the $2p^5 3d^{10}\,\underline{L}$ final state, where $2p^5$ denotes a Cu-$2p$ core hole and $\underline{L}$ denotes a p hole in the neighboring ligands, while the asymmetry of the main line and its large width were attributed to the bandwidth of the ligand p states.[6] It has been pointed out[7] that this interpretation is problematic in the case of the formally trivalent copper compound $NaCuO_2$ and probably also for doped high-T_c cuprates, where the $2p$ main line would be a two ligand-hole final state $2p^5 3d^{10}\underline{L}^2$. In $NaCuO_2$, for example, the Cu-$2p$ main line is found to be symmetric with a smaller width than usually observed for formally divalent copper compounds.[8]

However, in extending single-site approaches, recent calculations have shown that the ability of the system to screen the Cu-$2p$ core hole depends sensitively on the geometry and doping level of the CuO_2 network involved.[7] For typical cuprates such as La_2CuO_4, these calculations predict that the Cu-$2p$ XPS main line would be comprised of two peaks. The smaller, high binding-energy component is the $2p^5 3d^{10}\,\underline{L}$ final state, in which the Cu-$3d$ hole has moved to O-$2p$ orbitals of the same CuO_4 unit. The larger component at lower energy corresponds to a $2p^5 3d^{10}$ final state in which the hole is pushed out to reside mainly in the O-$2p$ orbitals of surrounding CuO_4 units, where it weakly interacts with the neighboring Cu spins, forming a so-called Zhang-Rice singlet.[9] It is the stability of this singlet that leads to the appearance of the $2p^5 3d^{10}$ final state at lowest binding energy.

There has been a discrepancy, however, between these calculations and what has been experimentally observed up to now in the undoped cuprates, namely that there has been no clear-cut double-peak structure seen for the Cu-$2p_{3/2,1/2}$ main lines. In addition, a recent theoretical study[10] of Cu-$2p$ photoelectron spectra for different CuO_2 systems has revealed effects of cluster size and dimensionality in the calculations. It has been shown by means of extended cluster calculations that the appearance of higher binding-energy features in the main line depends strongly on the actual size and coordination of the Cu_nO_m cluster.[10] It has also been pointed out that the previous interpretation of the two-component main line spectrum is related to the linear Cu_3O_{10} cluster used in Ref. 7.

The oxohalide compound studied in this paper, $Sr_2CuO_2Cl_2$, contains unbuckled CuO_2 planes, separated by two SrCl layers. It can be regarded as a model for a

two-dimensional Heisenberg antiferromagnet[11,12] and in particular as a model system for studying the dynamics of hole states created by photoemission in an antiferromagnetic background.[13] As the CuO_2 network is truly two-dimensional and the apical Cl ions have little influence on the electronic states close to the Fermi level, $Sr_2CuO_2Cl_2$ may also be a paradigm for the study of the electronic structure of CuO_2 planes and their response to the creation of core holes, in particular regarding the mechanisms of core hole screening. Thus its study may help to elucidate the electronic properties of the high-T_c cuprate compounds, which are believed to be determined by electronic states of the CuO_2 planes close to the Fermi level.

The organization of this paper is as follows. In Sec. II we briefly introduce the method of growing single crystalline $Sr_2CuO_2Cl_2$ and note some of its physical and structural properties which are relevant for later discussion. Section III contains a description of the experimental setup and Sec. IV introduces the cluster calculations. The experimental results are presented in Sec. V and are discussed in Sec. VI. Finally, a brief summary is given in Sec. VII.

II. SAMPLE PROPERTIES AND PREPARATION

$Sr_2CuO_2Cl_2$ is known to be highly resistive with a bandgap of about 1.7 eV.[14] It crystallizes in a body-centered-tetragonal structure of K_2NiF_4-type like La_2CuO_4.[15] In contrast to La_2CuO_4, no orthorhombic distortion is reported down to 10 K.[16] In addition, neither successful electron nor hole doping of $Sr_2CuO_2Cl_2$ has been reported so far. The lattice constants are $a=3.97$ Å and $c=15.61$ Å.[15] The distance Cu-Cl to the apical chlorine of 2.86 Å is much larger than the corresponding distance to the apical oxygen in La_2CuO_4 of 2.41 Å. The distance Cu-O of 1.99 Å is also larger than that of the in-plane Cu-O distance in La_2CuO_4 of 1.85 Å. The CuO_2 planes are separated by two SrCl units. From these interatomic distances we conclude that the electronic structure of the CuO_2 network of $Sr_2CuO_2Cl_2$ is more two-dimensional than that of La_2CuO_4.

Single crystalline $Sr_2CuO_2Cl_2$ is obtained basically following the method of Ref. 15. The crystals were grown by melting predried high-purity $SrCO_3$, $SrCl_2$, and CuO in the ratio of 1:1:1 at 1100°C in an alumina crucible. The temperature was decreased slowly at a rate of 3°/h down to 700 °C. Sheets of $Sr_2CuO_2Cl_2$ were present on the surface of the solidified melt. The samples used in this experiment were thin plates of $\sim 10\times 5\times 0.5$ mm^3.

The infrared and optical properties of $Sr_2CuO_2Cl_2$ have been examined recently.[14,17,18] From reflectivity spectra the effective negative charge on oxygen in $Sr_2CuO_2Cl_2$ was deduced and found to be the largest with regard to other cuprates studied.[17] This is possibly an indication of an increased ionic character of the Cu-O bonding in $Sr_2CuO_2Cl_2$.

III. EXPERIMENT

The x-ray photoemission experiments have been performed using a commercial XPS system[19] equipped with a standard Al Kα and Mg Kα x-ray twin anode as well as with a monochromated Al Kα source of 1486.6 eV photon energy. We used the monochromator for all photoelectron spectra presented here. The monochromated Al source is located perpendicular to the analyzer, the x-ray spot diameter is 2 mm. The probing spot of the analyzer was set to a diameter of about 0.7 mm, the entrance slit size being 4 mm. The full-cone angular resolution of the analyzer with the chosen slit sizes and electron optics is about 14°. The polar angle to the analyzer axis, θ, is always given with respect to the sample surface normal, i.e., $\theta=0°$ denotes normal emission. Due to geometric restrictions, like shadowing of the x rays, the useful polar angle range was about $20°\leqslant\theta\leqslant 70°$.

The energy resolution and the calibration of the system was determined using the photoemission lines of metallic Au, Ag, and Cu standards which were cleaned by means of Ar ion etching. The binding energy scale is always referred to the Fermi energy of Au, Ag, and Cu (set as zero) and to the binding energy of Ag-3$d_{3/2}$ (368.25 eV) and Au-4$f_{5/2}$ (84.0 eV). As $Sr_2CuO_2Cl_2$ is insulating, charging effects were observed resulting in a small shift of spectral features depending on the photon flux, without any influence on the shape of the spectra. The absolute energy scale has then been determined by the following means. The O-1s photoemission peak has been recorded for $\theta=20°$ with varying x-ray source power. The binding energy as a function of the x-ray power was obtained and then extrapolated to zero photon flux. The energy scale of the photoelectron spectra for different θ are obtained by shifting them to the extrapolated O-1s binding energy. The energy shift due to different charging of the sample did not exceed 0.3 eV between $\theta=20°$ and $\theta=60°$. We have also recorded the C-1s spectrum of surface hydrocarbon which could be observed as a very weak feature at the end of the measurements and was located at a binding energy of about 285 eV. We estimate the accuracy of the absolute energy calibration to be about ± 0.3 eV. One must keep in mind, though, that effects of sample charging may still be present in the photoelectron spectra due to possible instabilities in the photon flux of the x-ray anodes, which would lead to an additional broadening of the photoemission lines. We estimate this contribution to the experimental resolution for the spectra of the insulators to be small, since the width of the O-1s line was flux independent.

The energy resolution with the monochromated Al Kα excitation is about 0.4 eV for the chosen spectrometer pass energy of 6 eV, as estimated from the width of the Fermi edge of clean Ag. A constant as well as an integral background[20] have been subtracted from the photoelectron spectra.

The single crystalline samples were cleaved *in situ* under ultrahigh-vacuum conditions. No low-energy electron-diffraction (LEED) system is included in the setup of this XPS experiment, but the surface structure of $Sr_2CuO_2Cl_2$ has been checked in a different apparatus by cleaving the crystal under similar conditions. Clear and well defined LEED patterns consistent with a (001) surface with tetragonal symmetry were obtained. The base pressure of the XPS system was better than 1.0×10^{-8} Pa and the measurements were performed at room temperature. We observed that $Sr_2CuO_2Cl_2$ exhibits a remarkable inertness: no spectral changes in the Sr, Cl, O, and Cu core levels and the valence band were observed during a time scale of several days of continuous measurements.

IV. MODEL CALCULATION

To calculate the Cu-2p XPS, we use a two-dimensional Cu_5O_{16} cluster which consists of Cu-3$d_{x^2-y^2}$, O-2p_x, and 2p_y orbitals.[10] Basically, the Hamiltonian is that of the so-called d-p model. To include the core-hole effects in the photoemission final state, we also take into account the Coulomb interaction energy between 3d and core holes. The Hamiltonian in the hole picture is given by

$$H=\sum_{i,s}\varepsilon_d n_{d,is}+\sum_{j,\alpha,s}\varepsilon_p n_{p,j\alpha s}+\sum_i U_{dd}n_{d,i\uparrow}n_{d,i\downarrow}$$
$$+\sum_{\sigma}U_{dc}n_{d,k\sigma}n_{c,k}+\sum_{\langle i,j\rangle,\alpha,s}V_{pd,ij\alpha}(d^\dagger_{is}p_{j\alpha s}+p^\dagger_{j\alpha s}d_{is})$$
$$+\sum_{\langle j,j'\rangle,s}V_{pp,j\alpha j'\alpha'}(p^\dagger_{j\alpha s}p_{j'\alpha' s}+p^\dagger_{j'\alpha' s}p_{j\alpha s}), \qquad (1)$$

where $d^\dagger_{is}$ ($p^\dagger_{j\alpha s}$) creates a hole with spin s on the ith Cu-3$d_{x^2-y^2}$ orbital (the jth O-2p_α orbital with $\alpha=x$ or y).

The first and second terms on the right-hand side of Eq. (1) represent the one-electron single-particle energies, where $n_{d,is}$ ($n_{p,j\alpha s}$) is the number operator for the Cu-3d (O-2p_α) hole. We define the charge-transfer energy as $\Delta\equiv\varepsilon_p-\varepsilon_d$. The third term represents the Coulomb repulsion between Cu-3d holes. The fourth term represents the Coulomb potential between a core-hole and Cu-3d holes, with $n_{c,k}$ being the number operator for the core hole at site k. In the present study, k is taken at the central Cu site of the cluster. The fifth term represents the hybridization of the Cu-3d and O-2p orbitals, where $\langle i,j\rangle$ denotes the summation over the nearest-neighbor pairs. The last term represents the hybridization of the neighboring O-2p orbitals.

The typical values for the parameters involved in the above Hamiltonian are as follows: $pd\sigma=-1.5$ eV, $pp\sigma=1.0$ eV, $pp\pi=-0.3$ eV, $U_{dd}=8.8$ eV, $U_{\rm dc}=7.7$ eV, and $\Delta=3.5$ eV. They were derived from the first-principles calculation and some spectral analyses.[7,21] Among these parameters, Δ and $pd\sigma$ are crucial. Since the Cu-O distance in $Sr_2CuO_2Cl_2$ is somewhat longer than that in La_2CuO_4, a slightly smaller $pd\sigma$ may be better for $Sr_2CuO_2Cl_2$. In this study however, $pd\sigma$ is fixed to the above value for simplicity and the Δ dependence of the Cu-2p XPS is shown later.

The influence of core-hole creation can appear in the off-diagonal matrix elements of the Hamiltonian. For CuO, for example, it has been shown that the p-d hybridization strength in the photoemission final state reduces to 75% of the ground-state value on the basis of the first-principles calculation.[22] In the present study, we do not take into account this reduction effect. Instead, we note that this effect will make Δ smaller by about 1 eV.[23]

The Cu-2p XPS is calculated using the relation

$$I(E_B)=\mathrm{Im}\left\langle g\left| c_k\frac{1}{E_B-H+E_g}c_k^\dagger\right| g\right\rangle, \qquad (2)$$

as a function of binding energy E_B, where $c_k^\dagger$ creates a core hole at the kth Cu site and $|g\rangle$ and E_g are the wave function for the ground-state and the corresponding energy.

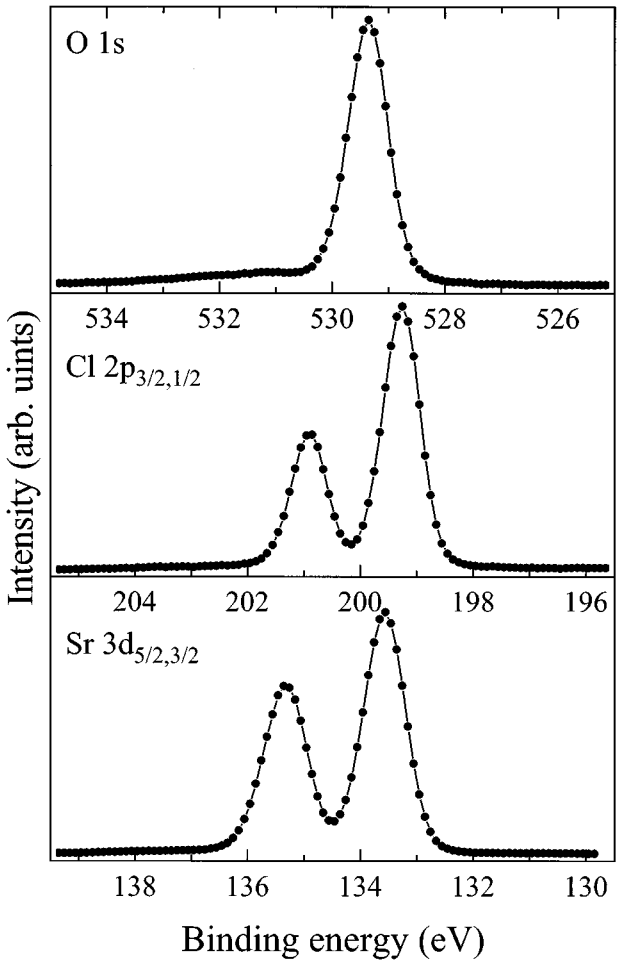

FIG. 1. From top to bottom: O-1s, Cl-2p, and Sr-3d photoelectron spectra of $Sr_2CuO_2Cl_2$ obtained with monochromated Al Kα excitation.

In this study, we use the Lanczos method to compute Eq. (2).[24] The obtained line spectrum is convoluted with Gaussian and Lorentzian functions with a total convolution width of 1.4 eV full width at half maximum (FWHM) to approximately match the experiment. Note that no multiplet splitting is included in this calculation.

V. EXPERIMENTAL RESULTS

A. Core-level spectra of O, Sr, and Cl

In Fig. 1 we show the O-1s, Cl-2p and Sr-3d photoelectron spectra taken at nearly normal emission with $\theta=20°$. The O-1s binding energy of about 529.3 eV is consistent with typical values for oxygen in other cuprate compounds.[25] The shape of the O-1s photoemission peak is highly symmetric and its FWHM is about 0.8 eV, which means a single component oxygen in the sample as is expected from the crystal structure. Virtually no oxygen contamination is present in the spectrum, which would lead to a feature at about 531–532 eV.[25] The shape of the O-1s spectrum did not change significantly with different θ, excluding contamination located on the sample surface.

The Cl-2p and the Sr-3d spectra also consist of very symmetric peaks, they exhibit only one doublet each, without signs of any further peaks due to contamination. The FWHM of the leading features of the Cl-2p and Sr-3d spectra are about 0.75 and 0.86 eV, respectively. The shape of these spectra were also θ independent. The binding energies of the Sr-3$d_{5/2}$ and Cl $2p_{3/2}$ photoemission lines of 133.6 and 199.3 eV, respectively, are consistent with an ionic Sr-Cl bond as anticipated from structural models: the Sr-3$d_{5/2}$ binding energy is intermediate in energy between that of Sr metal (134.2 eV) and of divalent SrO (132.6 eV).[26] From the core-level photoelectron spectra in Fig. 1 can be concluded that the samples under investigation are void of contamination within the detection limit of our method. A very small surface hydrocarbon feature at about 285 eV binding energy develops only after several days of continuous measurement.

A detailed analysis of the core-level photoemission intensities reveals not only important information about the sample quality but also as regards the terminating surface.[27] We can model the intensities of the different core-level spectra for the emission angle $\theta = 20°$ best if the sample surface is assumed to consist of mainly SrCl. This may also serve to explain the remarkable stability of the crystal surface of $Sr_2CuO_2Cl_2$, whereas most of the high-T_c compounds are notorious for their rapidly degrading surfaces.[25]

B. Cu-2p photoelectron spectrum

From polar angle-dependent XPS we can infer that the sample surface consists mainly of SrCl, whereas CuO_2 layers are mainly present in the bulk. This has important consequences in so far as the Cu and O spectra should then be representative of the bulk and all features should then be of intrinsic nature. We will discuss the possible influence of surface effects later in the context of the angular variation of the spectra and present here the Cu-2p XPS for nearly normal emission at $\theta = 20°$.

The Cu-$2p_{3/2,1/2}$ spin-orbit split main lines of $Sr_2CuO_2Cl_2$ are located at 933.5 and 953.5 eV, respectively. Both lines are accompanied by satellite features centered at 942.7 and 962.6 eV, respectively, which, as mentioned above, are interpreted as due to a poorly screened final state of predominantly $2p^5 3d^9$ character. In Fig. 2, the Cu-$2p_{3/2}$ part of the spectrum is presented. This spectrum differs from Cu-2p spectra of related cuprate compounds in two important aspects:

(1) The main line is clearly comprised of three distinct features labeled A, B, and C in the figure, and

(2) The satellite features are strong and exhibit a richer fine-structure compared to previous studies of cuprate compounds such as $YBa_2Cu_3O_{7-\delta}$ (Ref. 2), La_2CuO_4 (Refs. 3,28), CuO (Ref. 4), Sr_2CuO_3 (Ref. 23), Nd_2CuO_4 (Refs. 28,29) or $Bi_2Sr_2CaCu_2O_{8+\delta}$ (Ref. 30).

In other cuprate compounds, in particular in the structurally related La_2CuO_4, the Cu-2p main line is found to be a broad feature with a pronounced asymmetry on the higher binding-energy side of the spectrum. Some structure at the higher binding-energy side of the Cu-2p main line has been reported[31] in single-crystalline $Bi_2Sr_2CaCu_2O_{8+\delta}$, but compared to the spectrum in Fig. 2 the Cu-2p XPS of

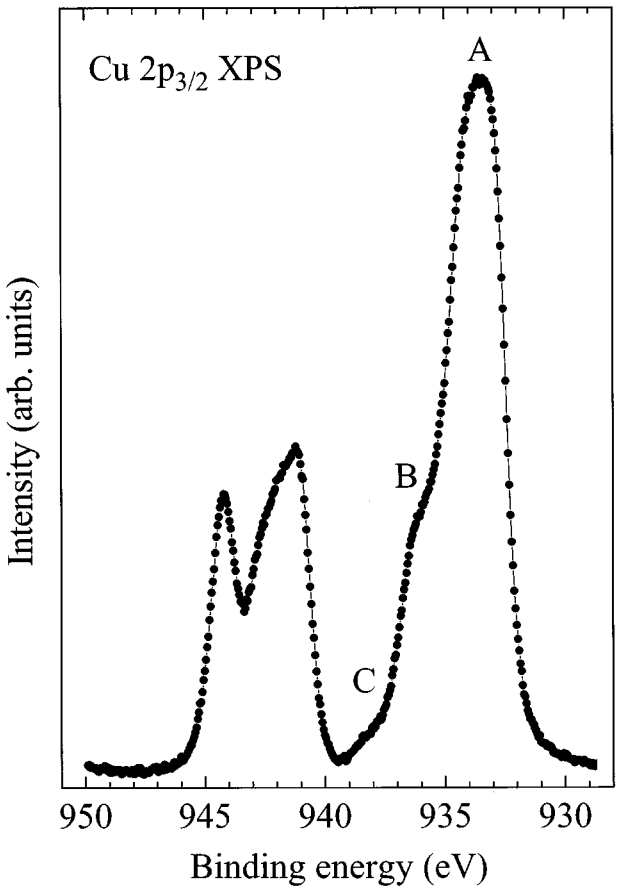

FIG. 2. Cu-$2p_{3/2}$ photoelectron spectrum with polar emission angle $\theta = 20°$. The spectrum consists of a broad main line at 933.5 eV and a strong satellite centered at about 943 eV. The main line is dominated by two features labeled A and B, which are due to well screened $2p^5 3d^{10}$ final states with different screening mechanisms, as discussed in the text in more detail. The satellite features are due a multiplet of the poorly screened $2p^5 3d^9$ final state.

$Bi_2Sr_2CaCu_2O_{8+\delta}$ differs much in shape as well as in the position of the feature B which is only weakly developed in $Bi_2Sr_2CaCu_2O_{8+\delta}$. Note also the very broad shape of feature A in $Sr_2CuO_2Cl_2$.

We estimate the intensity ratio I_B/I_A of the main line features by taking the peak areas from a fit using Voigt functions. We obtain $I_B/I_A \approx 0.3$. It is to be noted (see Sec. VI) that fitting feature A with only one peak does not lead to satisfying results: at least two peaks are needed. An additional structure at the lower binding-energy side of the main line has also been reported in $Bi_2Sr_2CaCu_2O_{8+\delta}$.[31] The weak feature C is located at about 938.3 eV with $I_C/I_A \approx 0.02$.

The satellite features between 940 and 945 eV in Fig. 2 contain more structure and do not have the rectangular shape usually observed in other cuprates. The intensity ratio $I_{\rm sat}/I_{\rm main}$ is about 0.50 and is thus considerably larger than that of La_2CuO_4 reported to be about 0.40–0.45.[3,28] The center of gravity of the satellite features is found to be located at about 9.2 eV higher binding energy than the main line peak maximum.

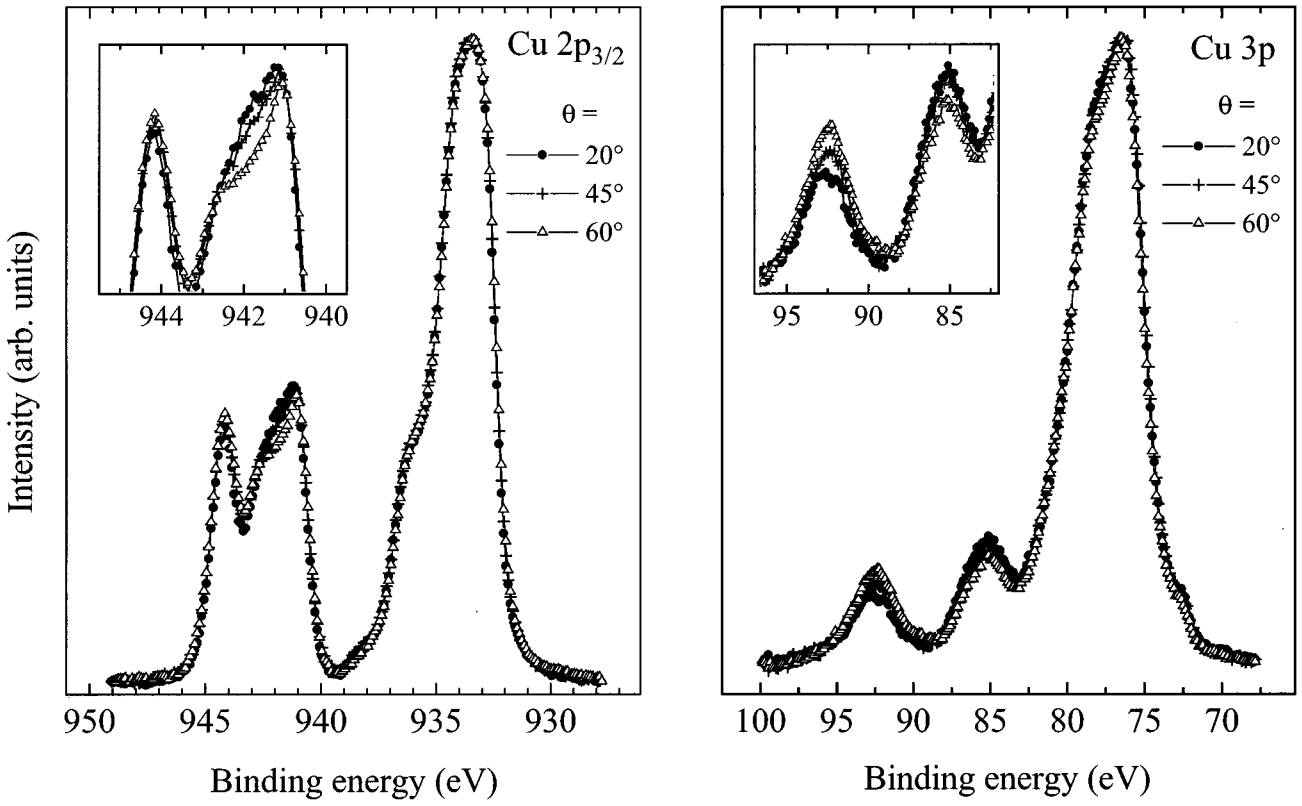

FIG. 3. Polar angle dependence of the Cu-$2p_{3/2}$ and the Cu-$3p$ photoelectron spectra. The peak maxima in each spectrum are set to unity and a constant as well as an integral background have been removed to obtain the same baseline before and after the core photoemission lines for all spectra. The insets show a blowup of the satellite part.

C. Polar angle dependence of the Cu-2*p* and 3*p* photoemission spectra

We observe strong angle-dependent effects in the satellites of the Cu-$2p_{3/2}$ (left part of Fig. 3) and Cu-$3p$ (right part of Fig. 3) photoelectron spectra, whereas the $2p_{1/2}$ part of the Cu-$2p$ spectrum is nearly angle independent (not shown). In order to compare the spectra more easily, a constant as well as an integral background have been removed from the spectra so to obtain equal intensities below and above the core-level photoemission lines and the spectra are normalized to the main peak maxima in each case. The insets of Fig. 3 show a blowup of the $2p^5 3d^9$ satellite part of the spectra. For the Cu-$2p_{3/2}$ satellites a systematic change in the spectral shape with the emission angle is clearly seen as an intensity decrease between $\sim$941–942 eV with increasing θ. The sharp feature at $\sim$944 eV does not change. For the Cu-$3p$ satellites, the peak height ratio between the feature at 85 and at 92.5 eV decreases systematically with increasing θ. It is remarkable that the shape of the Cu-$2p$ and $3p$ main line spectra is nearly angle independent.

D. Valence band

The valence-band spectrum of $Sr_2CuO_2Cl_2$ is presented in Fig. 4. The highest binding-energy part of the spectrum is dominated by emission from Cl-$3s$ and Sr-$3p$ shallow core-level states located at about 16.8 and 19.5 eV (not shown), respectively. We draw attention to the presence of a small feature at about 1.5 eV binding energy. It represents the first electron-removal state commonly accepted to be an antibonding Cu-$3d$–O-$2p$ A_{1g} singlet state[9] whose dispersion has been studied recently with angular-resolved photoemission.[13,32] Calculations for a Cu_2O_7 cluster predict that primarily an O-$2p$ electron would be removed from this state.[33] The features between $\sim$3 and $\sim$7 eV are due to hybridized Cu-O and Cl states. The spectrum of Fig. 4 is similar to previously published He I and II as well as VUV valence-band spectra.[32,34] Differences in intensities are related to cross-section effects, because using Al Kα excitation the photoionization cross sections of Cl-$3p$ and O-$2p$ are small compared to that of the Cu-$3d$ states.[35] The features between $\sim$10 and $\sim$14 eV are due to the poorly screened Cu-$3d^8$ final state.[4,33] From the energy difference between the main Cu-$3d$–O-$2p$ intensity and that of the Cl-$3p$ band of about 3 eV, one can infer a negligible contribution of Cl-$3p$ states to the electronic structure close to the Fermi level. Consequently, for the discussion of the different screening channels in the Cu-$2p$ photoemission, we therefore concentrate on the CuO_2 plane, only.

VI. DISCUSSION

A. Angle-dependent spectra

In the following, we discuss two possible scenarios responsible for the observed angular dependence in the Cu-$2p$ and $3p$ photoelectron spectra: one is a polarization effect of the bulk spectra, the other one is a surface-induced effect.

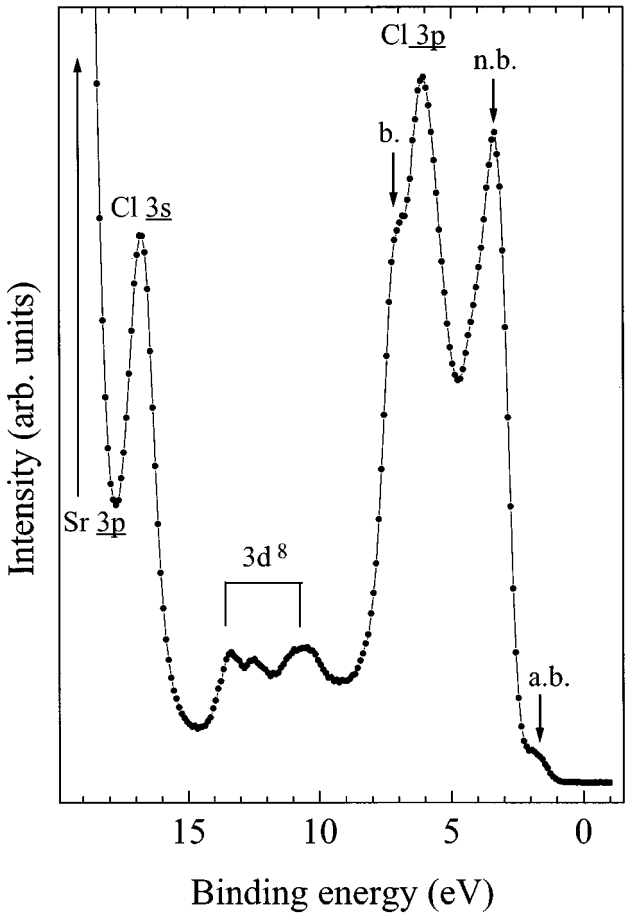

FIG. 4. Al Kα valence-band photoelectron spectrum of $Sr_2CuO_2Cl_2$ taken at an emission angle $\theta=20°$. The peak assignment of the different electron-removal states follows from the discussion in the text. The arrows indicate the positions of the bonding (b) nonbonding (nb), and antibonding (ab) Cu-3d–O-2p hybridized states.

The photoemission spectra shown in this paper are all taken with unpolarized radiation. Since the cleaved samples are layered and the 3d hole states have almost completely planar $3d_{x^2-y^2}$ character, a polarization effect in XPS can only be induced by the crystalline anisotropy of the sample. The crystal cleaves preferentially parallel to the ab plane. In the ideal situation, we vary, in changing the polar angle θ, the contribution of the electric-field vector $\vec{E}$ from lying exclusively in the ab plane for $\theta=90°$, to a situation in which $\vec{E}$ has additionally a nonvanishing component along the c axis for all other θ.

Calculations of the polarization-dependent Cu-2p and 3p XPS have been undertaken for La_2CuO_4.[36] A polarization effect can be induced via the multiplet splitting of those final states having an open 3d shell, this applies in particular to the Cu core-level satellites, as the core-hole interaction with the valence band is strong and the 3d hole states are highly anisotropic. The multiplet structure of these satellites is predicted to depend on the hybridization between different in-plane Cu-3d and O 2p states.[5] A polarization dependence is then caused by the different symmetries of the final states reached with $\vec{E}\perp c$ or $\vec{E}\parallel c$. The calculated polarization effects in the Cu np XPS occur mainly in the $np\rightarrow\epsilon s$ channel, whereas in the $np\rightarrow\epsilon d$ channel only a very small effect is predicted.[36] Since the cross section for the s channel is very small compared to the d channel for $\hbar\omega=1486.6$ eV, the polarization dependence is expected to be small in Cu-2p and 3p photoemission spectra using Al Kα excitation. Compared to the calculations of La_2CuO_4 the qualitative effect seen in the experimental spectra in Fig. 3 is well described by the theory.[36] But the magnitude of the effects seen in $Sr_2CuO_2Cl_2$ appears to be more than an order of magnitude larger than calculated for La_2CuO_4.

An important aspect of the second scenario is that the crystal-field splitting close to the surface may be different from the bulk, thus inducing a different multiplet splitting for near-surface layers than for truly bulk layers. These effects are probably small, since CuO_2 is not at the surface, and it is at present unclear, as to whether a change in the Madelung potentials could produce such strong effects. Nevertheless, we consider it to be more likely that our result for $Sr_2CuO_2Cl_2$ indicates the surface sensitivity of the satellite features. Since the multiplet structure is sensitive to crystal-field splittings in general, the energy levels of $3d_{3z^2-r^2}$, $3d_{xy}$, $3d_{yz}$, and $3d_{xz}$ relative to $3d_{x^2-y^2}$ are changed somewhat for surface and bulk. From this point of view it is questionable whether polarization effects possibly present in the bulk can be observed in planar CuO_2 systems at all using surface sensitive methods, because the presence of a terminating surface with broken translational symmetry in principle affects the crystal-field splitting in the way described above. To our knowledge, only few XPS experiments on cuprate single crystals are reported (see, for example, Refs. 31 and 37) without showing angular-dependent Cu core-level spectra, so the clarification of this matter has to be postponed. We conclude this section by noting the fact that the shape of the Cu-2p main line is angle independent is fully consistent with the assignment of the Cu-2p main line features to the final-state configuration $2p^5 3d^{10}$ with a closed 3d shell.

B. Cu-2p spectrum

We now discuss the shape of the Cu-2p main line, in particular the feature A, in more detail. As already mentioned, this feature is very broad and appears to be comprised of more than one peak. A reasonable fit of the Cu-2p main line can only be achieved if the main line as a whole consists of at least three features. This is shown in Fig. 5, where a set of three Voigt functions are used. The weak feature C located at about 938 eV is not included in this fit for reasons of simplicity. The Gaussian part of the FWHM has been fixed to $\sim$0.45 eV in order to match approximately the experimental resolution, the Lorentzian part is allowed to vary freely. The parameters obtained for the different peaks are summarized in Table I.

In Fig. 6 we show the calculated Cu-2p photoelectron spectra as a function of Δ, keeping $\Delta-U_{dc}=-4.2$ eV so as not to change the energy separation of the main line to the satellite. Since the height of the main peak is normalized to unity in this figure, the satellite intensity increases with increasing Δ. This is mainly because the $3d^9$ weight in the ground-state wave function increases with Δ. With increasing Δ, a shoulder grows up at the higher binding-energy side

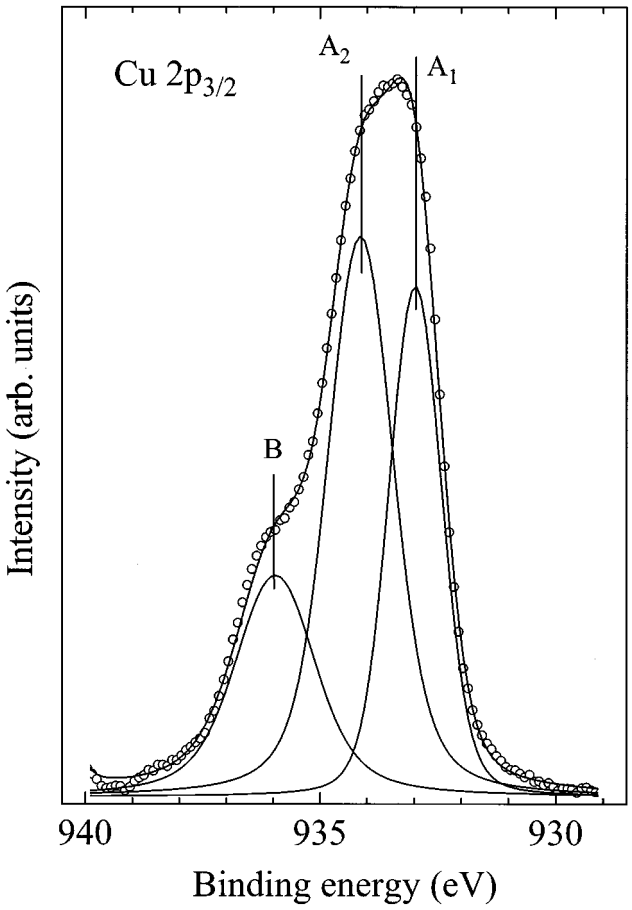

FIG. 5. The Cu-2$p_{3/2}$ main line (experiment: dots) fitted with three Voigt functions (solid lines). The line connecting the experimental points is the fit. The fit parameters are summarized in Table I. Note, that it is impossible to fit A with only one Voigt function with reasonable parameters.

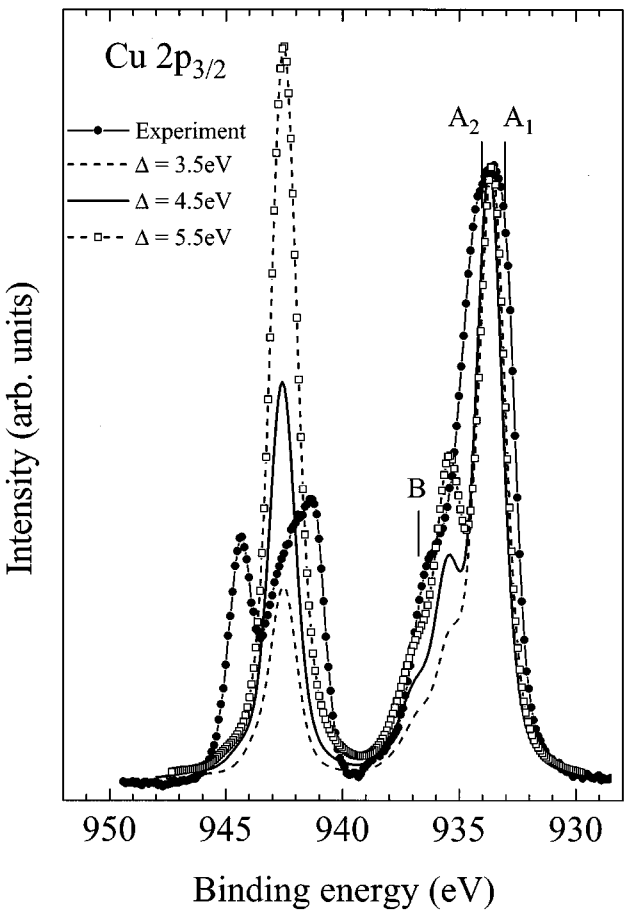

FIG. 6. Comparison of the experimental photoelectron spectrum with the calculated Cu-2$p_{3/2}$ spectrum using different Δ. In the calculation $\Delta - U_{dc}$ has been kept constant and the convolution width is 1.4 eV. See text for more details.

of the leading peak. Since multiplet splitting has not been included in the calculation the satellite part of the spectrum appears as only one line.

In comparison with the experiment, some serious limitations of the calculation are to be noted, which are in the first place its inability to reproduce neither the shape of the main line nor the energy separations of B relative to A correctly. The energy separation $\Delta E_{A,B}$ between the two calculated main line features is much smaller than the energy difference between features A and B. As $\Delta E_{A,B}$ is sensitive to the hopping matrix elements $pd\sigma$, $pp\sigma$, and $pp\pi$, the parameter set used for this calculation, in particular the hopping matrix elements, should be adjusted consistently. This may introduce even more difficulties, as the proper reduction of the direct hopping matrix elements due to the larger Cu-O bonding distance in $Sr_2CuO_2Cl_2$ compared to La_2CuO_4 would further reduce instead of increase the energy separation between the two features.

TABLE I. Parameters of the Cu-2p main line fit of Fig. 5.

	Energy (eV)	Area relative to A_1	FWHM (eV)
A_1	932.97	1.00	1.32
A_2	934.14	1.45	1.65
B	935.96	0.72	2.03

The calculated Cu-2p main line spectrum consists of a complex structure with two intense features. This prominent double-peak feature of the main structure originates from the p-d hybridization in the CuO_4 units surrounding the core hole site. The leading peak in the calculations in Fig. 6 corresponds to the nonlocal screening channel where a hole pushed away from the core-hole site moves to the neighboring CuO_4 units to form a Zhang-Rice singlet.[9] The shoulder peak in the calculations corresponds to the local screening channel where a pushed out hole interacts only weakly with the Cu-3d holes and screening takes place mainly through the O-2p bands. Therefore the energy separation between the leading peak and the shoulder approximately corresponds to the Zhang-Rice singlet formation energy, which is sensitive to $pd\sigma$. As Δ is increased, the formation probability of the Zhang-Rice singlet is so suppressed that the leading peak becomes weak, compared with the shoulder. The intensity of the shoulder is thus sensitive to Δ. Among the calculated results shown in Fig. 6 the case of a fairly large $\Delta = 4.5$ eV approximates the experimental spectrum of $Sr_2CuO_2Cl_2$ best. A similar conclusion concerning Δ can be drawn from the ratio of the satellite to the main line intensity I_{sat}/I_{main},

which is about 0.5 in $Sr_2CuO_2Cl_2$. The calculation gives $I_{sat}/I_{main}=0.5$, in good agreement with the experiment. For the related system La_2CuO_4 as well as for the Nd_2CuO_4, I_{sat}/I_{main} is considerably smaller;[38] thus a larger Δ in $Sr_2CuO_2Cl_2$ than in the forementioned cuprates is reasonable.

It is tempting to shift the calculated main line spectrum so that the leading peak and the shoulder feature coincide with A_1 and A_2, respectively. The double-peak character of feature A is most clearly seen in the related oxochloride compound $Ba_2Cu_3O_4Cl_2$ whose Cu_3O_4 plane contains, besides the cupratelike CuO_2 subsystem, an extra Cu site.[39] Hopping from this extra Cu site can only occur mediated by 90° Cu-O-Cu interactions. This means that core holes located at the extra Cu site can only be screened locally since delocalization of the $3d$ valence-band hole through the Zhang-Rice screening channel is not possible. Consequently the intensity of feature A_2 is much larger than A_1. Details of this will be published elsewhere.

In the model of van Veenendaal *et al.*[7] based on calculations of a linear cluster, the main line, i.e., the lowest binding energy feature, is the $2p^53d^{10}$ final state where only $3d_{x^2-y^2}$ states participate. We assign feature A_1 to this nonlocal screening process. All higher binding-energy features, A_2 and B, etc., would thus be ''excited'' states due to local screening channels. We assume that the restriction to a two-band model (O-$2p_{x,y}$ and Cu-$3d_{x^2-y^2}$) is only a starting point to understand the gross features of the spectrum. Further $3d$ states, i.e., $3d_{3z^2-r^2}$, and O-$2p_z$ states presumably have to be taken into account for a more complete description. It is also to be noted that the triple-peaked main line can be a consequence of the CuO_2 network dimensionality, as has been shown by multiple-site cluster calculation.[10]

Finally, we briefly discuss the Cu-$2p_{3/2}$ satellite features. The multiplet structure in the $2p^53d^9$ final state has been calculated in the past for La_2CuO_4.[5] The shape of the $2p^53d^9$ spectrum was found to be dependent on the hybridization of Cu-$3d_{x^2-y^2}$ and Cu-$3d_{xy}$ states with O-$2p_x,2p_y$ states. In case of La_2CuO_4 it has been demonstrated that the typical squarish shape of the multiplet-split $2p^53d^9$ final state observed in many cuprates is related to an anisotropic hybridization of the in-plane Cu-$3d$–O-$2p$ states with b_{1g} and b_{2g} symmetry.[5] Instead, the shape of the Cu-$2p_{3/2}$ satellite features in $Sr_2CuO_2Cl_2$ most closely resembles that case calculated for La_2CuO_4, in that the Cu-$3d$–O-$2p$ hybridization is isotropic.[5] This agrees with the general picture that can be derived from our experiments as well as from optical data[17] insofar as the bonding character of Cu-O in $Sr_2CuO_2Cl_2$ is more ionic than in La_2CuO_4. In more ionic compounds the atomic multiplet splitting is expected to be more important than solid-state hybridization effects.

VII. SUMMARY AND CONCLUSIONS

We conclude that the cleavage of $Sr_2CuO_2Cl_2$ resulted in a well defined surface in which CuO_2 layers are not dominating. We found that the sample was nearly free of contamination and the photoemission spectra shown are related to intrinsic properties of $Sr_2CuO_2Cl_2$. Since $Sr_2CuO_2Cl_2$ cannot easily be doped, we believe the spectral features shown in this paper to be characteristic of antiferromagnetic, insulating planar CuO_2 systems.

The Cu-$2p$ spectrum taken with high-resolution XPS shows some very remarkable features, namely a multicomponent main line and a large satellite intensity. The shape of the satellite part of the Cu-$2p$ spectrum differs considerably from the spectra of other cuprates known so far. The features in the main line are discussed in the context of nonlocal and local screening mechanisms. The lowest energy component of the Cu-$2p$ main line, denoted by A_1, is a $2p^53d^{10}$ final state with Zhang-Rice singlet screening, whereas the higher binding energy features, denoted by A_2 and B, probably are due to local screening channels involving O-$2p_{x,y}$ states. The limitations of the present calculation and probably of the d-p model in general are to be noted, which in the first place entail the failure to reproduce the shape of feature A as well as the energy separation of A and B. Size effects and the dimensionality of the CuO_2 network have probably to be included for a better theoretical description.

We observe clear angular-dependent Cu-$2p$ and $3p$ core-level satellites, the origin of these effects is at present unclear. We assume surface effects to be the most likely reason for this, although CuO_2 layers do not tominate the cleavage surface. This would have some implications for the attempt to study bulk polarization effects by using surface sensitive spectroscopic techniques as XPS, because it would appear to be difficult if not impossible to avoid surface effects. From the absence of any polar angle effects in the Cu-$2p$ main line we can deduce a closed $3d$ shell configuration for all main line features.

ACKNOWLEDGMENTS

T.B. is grateful to S. L. Drechsler, K. Maiti, and S. R. Barman for extensive and valuable discussions. M.S.G. thanks the European Union for financial support under the HCM program. Part of this work was supported by the Bundesministerium für Bildung, Wissenschaft, Forschung und Technologie (BMBF) under Contracts No. 05-605 BDA and 13N6599/9.

*Electronic address: tboeske@ifw-dresden.de

[1] G. van der Laan, C. Westra, C. Haas, and G. A. Sawatzky, Phys. Rev. B **23**, 4369 (1981).
[2] A. Fujimori, E. Takayama-Muromachi, Y. Uchida, and B. Okai, Phys. Rev. B **35**, 8814 (1987).
[3] N. Nücker, J. Fink, B. Renker, D. Ewert, C. Politis, P. J. W. Weijs, and J. C. Fuggle, Z. Phys. B **67**, 9 (1987).
[4] J. Ghijsen, L. H. Tjeng, J. van Elp, H. Eskes J. Westerink, G. A. Sawatzky, and M. T. Czyzyk, Phys. Rev. B **38**, 11 322 (1988).
[5] K. Okada and A. Kotani, J. Phys. Soc. Jpn. **58**, 2578 (1989).
[6] O. Gunnarsson and K. Schönhammer, Phys. Rev. B **28**, 4315 (1983).
[7] M. A. van Veenendaal, H. Eskes, and G. A. Sawatzky, Phys. Rev. B **47**, 11 462 (1993).
[8] T. Mizokawa, A. Fujimori, H. Namatame, K. Akeyama, and N. Kosugi, Phys. Rev. B **49**, 7193 (1994).
[9] F. C. Zhang and T. M. Rice, Phys. Rev. B **37**, 3759 (1988).
[10] K. Okada and A. Kotani, Phys. Rev. B **52**, 4794 (1995).

[11] M. Greven, R. J. Birgeneau, Y. Endoh, M. A. Kastner, B. Keimer, M. Matsuda, G. Shirane, and T. R. Thurston, Phys. Rev. Lett. **72**, 1096 (1994).
[12] B. J. Suh, F. Borsa, L. L. Miller, M. Corti, D. C. Johnston, and D. R. Torgeson, Phys. Rev. Lett. **75**, 2212 (1995).
[13] B. O. Wells, Z.-X. Shen, A. Matsuura, D. M. King, M. A. Kastner, M. Greven, and R. J. Birgeneau, Phys. Rev. Lett. **74**, 964 (1995).
[14] J. D. Perkins, J. M. Graybeal, M. A. Kastner, R. J. Birgeneau, J. P. Falck, and M. Greven, Phys. Rev. Lett. **71**, 1621 (1993).
[15] L. L. Miller, X. L. Wang, S. X. Wang, C. Stassis, D. C. Johnston, J. Faber, Jr., and C.-K. Loong, Phys. Rev. B **41**, 1921 (1990).
[16] D. Vaknin, S. K. Sinha, C. Stassis, L. L. Miller, and D. C. Johnston, Phys. Rev. B **41**, 1926 (1990).
[17] S. Tajima, S. Uchida, S. Ishibashi, T. Ido, H. Takagi, T. Arima, and Y. Tokura, Physica C **168**, 117 (1990).
[18] A. Zibold, H. L. Liu, S. W. Moore, J. M. Graybeal, and D. B. Tanner, Phys. Rev. B **53**, 11 734 (1996).
[19] PHI 5600 of Perkin-Elmer Corporation, Eden Prairie, Minnesota 55344.
[20] S. Tougaard, Surf. Sci. **216**, 343 (1989).
[21] M. S. Hybertsen, M. Schlüter, and N. E. Christensen, Phys. Rev. B **39**, 9028 (1989).
[22] K. Karlsson, O. Gunnarsson, and O. Jepsen, J. Phys. Condens. Matter **4**, 2801 (1992).
[23] K. Okada, A. Kotani, K. Maiti, and D. D. Sarma, J. Phys. Soc. Jpn. **65**, 1844 (1996).
[24] See, for example, V. Heine, *Solid State Physics: Advances in Research and Applications*, edited by H. Ehrenreich, F. Seitz, and D. Turnbull (Academic, New York, 1980), Vol. 35, p. 87.
[25] R. P. Vasquez, J. Electron Spectrosc. Relat. Phenom. **66**, 209 (1994).
[26] R. P. Vasquez, J. Electron Spectrosc. Relat. Phenom. **66**, 241 (1994).
[27] P. A. P. Lindberg, I. Lindau, and W. E. Spicer, Phys. Rev. B **40**, 6822 (1989)>
[28] J. M. Tranquada, S. M. Heald, W. Kunnmann, A. R. Moodenbaugh, S. L. Qiu, Y. Xu, and P. K. Davies, Phys. Rev. B **44**, 5176 (1991).
[29] T. R. Cummins and R. G. Egdell, Phys. Rev. B **48**, 6556 (1993).
[30] Z.-X. Shen, P. A. P. Lindberg, B. O. Wells, D. B. Mitzi, I. Lindau, W. E. Spicer, and A. Kapitulnik, Phys. Rev. B **38**, 11 820 (1988).
[31] F. Parmigiani, Z. X. Shen, D. B. Mitzi, I. Lindau, W. E. Spicer, and A. Kapitulnik, Phys. Rev. B **43**, 3085 (1991).
[32] J. J. M. Pothuizen, R. Eder, N. T. Hien, M. Matoba, A. A. Menovsky, and G. A. Sawatzky, Phys. Rev. Lett. **78**, 717 (1997).
[33] H. Eskes and G. A. Sawatzky, Phys. Rev. B **43**, 119 (1991).
[34] A. Fujimori, Y. Tokura, H. Eisaki, H. Takagi, S. Uchida, and M. Sato, Phys. Rev. B **40**, 7303 (1989).
[35] J. J. Yeh and I. Lindau, At. Data Nucl. Data Tables **32**, 1 (1985).
[36] K. Okada, A. Kotani, B. T. Thole, and G. A. Sawatzky, Solid State Commun. **76**, 1277 (1990).
[37] Z.-X. Shen, R. S. List, D. S. Dessau, F. Parmigiani, A. J. Arko, R. Bartlett, B. O. Wells, I. Lindau, and W. E. Spicer, Phys. Rev. B **42**, 8081 (1990).
[38] F. Parmigiani and L. Sangaletti, J. Electron Spectrosc. Relat. Phenom. **66**, 223 (1994).
[39] O. Knauff, T. Böske, M. Knupfer, M. S. Golden, G. Krabbes, and J. Fink, J. Low Temp. Phys. **105**, 353 (1996).